Inorganic Chemistry

Article

pubs.acs.org/IC

Improvement of Green Upconversion Monochromaticity by Doping Eu^{3+} in Lu_2O_3:Yb^{3+}/Ho^{3+} Powders with Detailed Investigation of the Energy Transfer Mechanism

Guotao Xiang,*[,†] Yan Ma,[†] Wen Liu,[‡,§] Sha Jiang,[†] Xiaobing Luo,[†] Li Li,[†] Xianju Zhou,[†] Zhiwei Gu,[†] Jiapeng Wang,[†] Yongshi Luo,[‡] and Jiahua Zhang*[,‡]

[†]Department of Mathematics and Physics, Chongqing University of Posts and Telecommunications, 2 Chongwen Road, Chongqing 400065, People's Republic of China

[‡]State Key Laboratory of Luminescence and Applications, Changchun Institute of Optics, Fine Mechanics and Physics, Chinese Academy of Sciences, 3888 Eastern South Lake Road, Changchun 130033, People's Republic of China

[§]Graduate School of Chinese Academy of Sciences, Beijing 100039, People's Republic of China

Supporting Information

ABSTRACT: The monochromaticity improvement of green upconversion (UC) in Lu_2O_3:Yb^{3+}/Ho^{3+} powders has been successfully realized by tridoping Eu^{3+}. The integral area ratio of green emission to red emission of Ho^{3+} increases 4.3 times with increasing Eu^{3+} doping concentration from 0 to 20 mol %. The energy transfer (ET) mechanism in the Yb^{3+}/Ho^{3+}/Eu^{3+} tridoping system has been investigated carefully by visible and near-infrared (NIR) emission spectra along with the decay curves, revealing the existence of ET from the Ho^{3+} $^5F_4/^5S_2$ level tothe Eu^{3+} $^5D_0$ level and ET from the Ho^{3+} $^5I_6$ level to the Eu^{3+} $^7F_6$ level. In addition, the population routes of the red-emitting Ho^{3+} $^5F_5$ level in the Yb^{3+}/Ho^{3+} codoped system under 980 nm wavelength excitation have also been explored. The ET process from the Yb^{3+} $^2F_{5/2}$ level to the Ho^{3+} $^5I_7$ level and the cross-relaxation process between two nearby Ho^{3+} ions in the $^5F_4/^5S_2$ level and $^5I_7$ level, respectively, have been demonstrated to be the dominant approaches for populating the Ho^{3+} $^5F_5$ level. The multiphonon relaxation process originating from the Ho^{3+} $^5F_4/^5S_2$ level is useless to populate the Ho^{3+} $^5F_5$ level. As the energy level gap between the Ho^{3+} $^5I_7$ level and Ho^{3+} $^5I_8$ level matches well with that between Eu^{3+} $^7F_6$ level and Eu^{3+} $^7F_0$ level, the energy of the Ho^{3+} $^5I_7$ level can be easily transferred to the Eu^{3+} $^7F_6$ level by an approximate resonant ET process, resulting in a serious decrease in the red UC emission intensity. Since this ET process is more efficient than the ET from the Ho^{3+} $^5F_4/^5S_2$ level to the Eu^{3+} $^5D_0$ level as well as the ET from the Ho^{3+} $^5I_6$ level to the Eu^{3+} $^7F_6$ level, the integral area ratio of green emission to red emission of Ho^{3+} has been improved significantly.

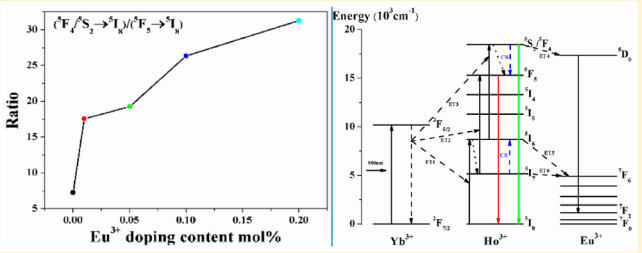

INTRODUCTION

Today, luminescent materials doped with combinations of trivalent rare earth ions, such as Yb^{3+}/Er^{3+}, Yb^{3+}/Ho^{3+}, and Yb^{3+}/Tm^{3+}, have raised concern about their UC properties, which can emit ultraviolet (UV) or visible photons under the excitation of NIR light.[1−3] In contrast with the conventional downconversion materials, such as organic dyes and quantum dots (QDs), UC materials own large anti-Stokes shift narrow emission, long luminescence lifetime, outstanding photostability, and low background noise.[4−7] More importantly, previous research has provided evidence that the UC materials with appropriate surface modification are less toxic to cells and tissues than those of organic dyes and QDs.[8] The unique physicochemical properties and inherent optical properties make them suitable for applications in fields such as photonics, photovoltaics, 3-D displays, optical encoding, and bioimaging.[9−11]

Nevertheless, the abundant metastable states of rare earth ions usually give rise to multicolor emission bands simultaneously under NIR excitation, which seriously hinders the utilization of UC phosphors in relevant areas: for instance, the quantitative imaging of cells and tissues labeled with multiple UC probes.[12] Up to now, great efforts have been given to the development of high chromatic purity UC emission. As examples, Hao et al. have obtained large red emission to green emission ratio along with remarkable UC enhancement in α-$NaYF_4$:Yb^{3+}/Er^{3+} through transition metal ion Mn^{2+} tridoping and Zhang and his group improved the green UC emission monochromaticity of Ho^{3+} in Y_2O_3:Yb^{3+}/Ho^{3+} by doping trivalent rare earth ions Eu^{3+}.[13,14] From these, it can be seen that utilizing ET processes to selectively populate specific energy levels of activators through rare earth ion or transition metal ion tridoping is a feasible approach to improve the UC monochromaticity.

Received: May 13, 2017
Published: July 12, 2017

DOI: 10.1021/acs.inorgchem.7b01236
Inorg. Chem. 2017, 56, 9194−9199

Of a variety of UC materials, β-$NaYF_4$ and β-$NaLuF_4$ are acknowledged as the most two efficient matrixes.[15−17] Benefiting from their low photon energy (~360 cm^{-1}), the nonradiative relaxation phenomena can be dramatically reduced during the ET processes, which results in high UC quantum yields. However, the applications of fluoride UC materials are restricted by some disadvantages, such as poor chemical stability, complex synthetic processes, certain toxicity to human bodies, and so on. In comparison to fluoride materials, oxide materials possess extreme physicochemical stability and a simple synthetic process.[18] For the past few years, a great number of studies have been dedicated to exploit effective UC oxide hosts.[19−21] Among the various UC oxide hosts, Y_2O_3 has long been considered as the representative oxide UC matrix with highly efficient UC emission.[22] Nevertheless, Zhang et al. and Capobianco et al. have demonstrated that the trivalent rare earth ion doped Lu_2O_3 phosphors show stronger UC intensity in comparison to that found in Y_2O_3 phosphors, respectively, resulting from the unique electronic state at the top of the valence of lutetium.[23,24] Similar conclusions have also been verified between β-$NaYF_4$ and β-$NaLuF_4$ and between YF_3 and LuF_3.[25,26] So far, however, there have not been very many explorations concerning the UC properties in the Lu_2O_3 host, especially the UC monochromaticity improvement.

In the present work, the green UC monochromaticity improvement has been realized by Eu^{3+} doping in Lu_2O_3:Yb^{3+}/Ho^{3+} phosphors. As Eu^{3+} doping concentration increases from 0 to 20 mol %, the integral area ratio of green emission to red emission of Ho^{3+} increases 4.3-fold. On the basis of an analysis of the steady state fluorescence spectra and the decay curves, the ET mechanisms in the Yb^{3+}/Ho^{3+}/Eu^{3+} tridoping system have been explored in detail. Meanwhile, the population routes of the red-emitting Ho^{3+} $^5F_5$ level in a Yb^{3+}/Ho^{3+} codoped system under 980 nm wavelength excitation have been investigated. The results show that the main approaches for populating the Ho^{3+} $^5F_5$ level are the ET process from the Yb^{3+} $^2F_{5/2}$ level to Ho^{3+} $^5I_7$ level and the cross-relaxation process between two nearby Ho^{3+} ions in the $^5F_4/^5S_2$ level and $^5I_7$ level, respectively. In addition, the reason for the green UC monochromaticity improvement has also been discussed.

EXPERIMENTAL SECTION

Chemicals. SpecPure grade rare earth oxides (Lu_2O_3, Yb_2O_3, Ho_2O_3, Eu_2O_3, 99.99%), supplied by Yangkou state-run rare earth company, were employed as the raw materials without further purification.

Synthesis of Lu_2O_3:20 mol % Yb^{3+}/1 mol % Ho^{3+}/x mol % Eu^{3+} (x = 0, 1, 5, 10, 20). A conventional high-temperature solid state method was used to prepare the Lu_2O_3:20 mol % Yb^{3+}/1 mol % Ho^{3+}/x mol % Eu^{3+} powder samples. First, the raw materials Lu_2O_3 (99.99%), Yb_2O_3 (99.99%), Ho_2O_3 (99.99%), and Eu_2O_3 (99.99%) were comibned in an agate mortar and then mixed homogeneously for 1.5 h. Finally, the powders were placed in an alumina crucible with a lid and sintered in a box furnace at 1550 °C for 5 h in air.

Characterization. Powder X-ray diffraction (XRD) data were collected by Cu Kα radiation (λ = 1.54056 Å) on a Bruker D8 advance diffractometer. The visible and NIR spectra were detected using a FLS920 spectrometer purchased from Edinburgh Instruments. A Tektronix digital oscilloscope (TDS 3052) equipped with an optical parametric oscillator (OPO) as the excitation source was employed to measure the decay curves. The lifetime value of each decay curve was obtained by integrating the area under the corresponding normalized lifetime curve.

RESULTS AND DISCUSSION

Structure. Figure 1 shows the XRD patterns of Lu_2O_3:Yb^{3+}/Ho^{3+}/Eu^{3+} powders as a function of Eu^{3+} doping concentration. The main features of the diffraction peaks, including positions and relative intensity, possess the characteristics of cubic Lu_2O_3, corresponding to the standard card JCPDS 43-1021. Moreover, no other phase is detected with increasing Eu^{3+} concentration in the XRD patterns, demonstrating a high concentration of Eu^{3+} dopant has no effect on the crystal formation and transition. However, as the Eu^{3+} doping concentration increases, the diffraction peaks shift slightly to low angles, implying the expansion of lattice constants and unit-cell volumes, which arises from the substitution of the larger Eu^{3+} (1.206 Å) for the smaller Lu^{3+} (1.117 Å). Table 1 shows the lattice constants and unit-cell volumes of the samples with different Eu^{3+} concentrations, which are calculated from the XRD data.

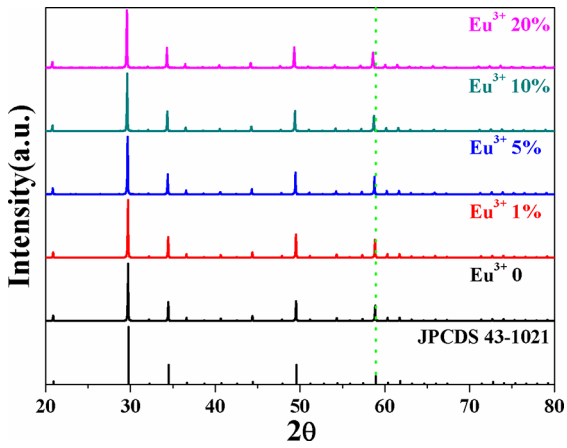

Figure 1. XRD patterns of Lu_2O_3:Yb^{3+}/Ho^{3+}/Eu^{3+} powders as a function of Eu^{3+} doping concentration with the standard XRD data of cubic Lu_2O_3.

Table 1. Lattice Constants and Unit-Cell Volumes of Lu_2O_3:Yb^{3+}/Ho^{3+}/Eu^{3+} Powders as a Function of Eu^{3+} Doping Concentration

concn of Eu^{3+} (%)	a (Å)	cell volume (Å^3)
0	10.4040	1126.16
1	10.4075	1127.30
5	10.4224	1132.15
10	10.4375	1137.08
20	10.4503	1141.26

Luminescence Properties. The UC spectra of the samples doped with different Eu^{3+} contents excited by 980 nm wavelength at low-output power density are measured and depicted in Figure 2. The spectra are all normalized to the maximum intensity of the $^5F_4/^5S_2 \rightarrow {}^5I_8$ transition. For the product without Eu^{3+} content, the UC spectrum includes two distinct emission bands in the range of 500−700 nm. The green emission band located at 550 nm belongs to the $^5F_4/^5S_2 \rightarrow {}^5I_8$ transition of Ho^{3+}, and the red emission band peak at around 670 nm is attributed to the $^5F_5 \rightarrow {}^5I_8$ transition of Ho^{3+}. A weak emission peak located at 611 nm appears in the as-prepared samples doped with Eu^{3+}, which is assigned to the $^5D_0 \rightarrow {}^7F_2$ transition of Eu^{3+}. Although the UC intensity of the as-prepared

DOI: 10.1021/acs.inorgchem.7b01236
Inorg. Chem. 2017, 56, 9194−9199

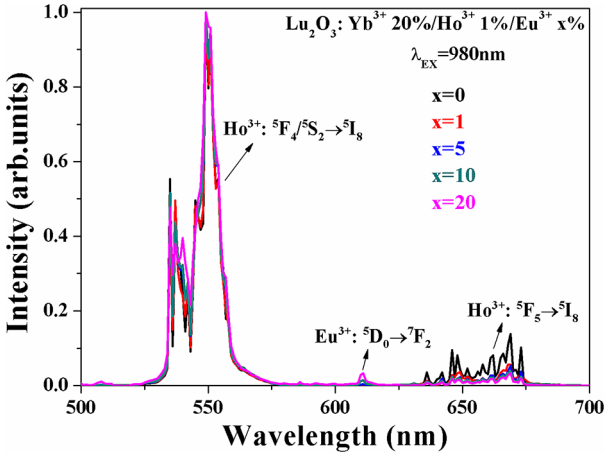

Figure 2. Normalized UC spectra of Lu_2O_3:Yb^{3+}/Ho^{3+}/Eu^{3+} powders with different Eu^{3+} concentrations under 980 nm wavelength excitation at low-output power density.

samples is reduced with an increase in Eu^{3+} content (see Figure S1 in the Supporting Information), the integral area ratio of the $^5F_4/^5S_2 \rightarrow {}^5I_8$ transition (integrating from 525 to 575 nm) to the $^5F_5 \rightarrow {}^5I_8$ transition (integrating from 625 to 675 nm) of Ho^{3+} increases 4.3 times, as shown in Figure 3, which means

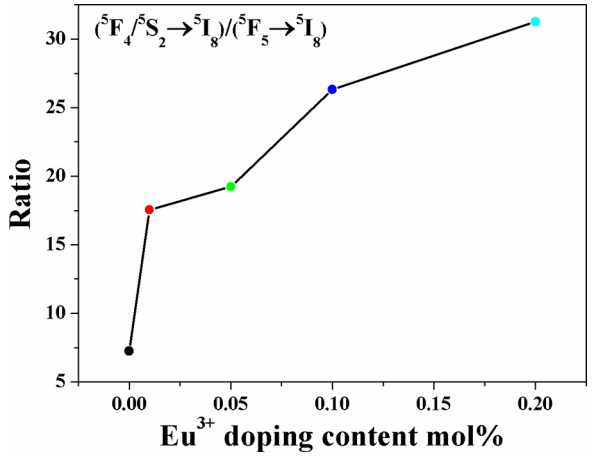

Figure 3. Integral area ratio of the $^5F_4/^5S_2 \rightarrow {}^5I_8$ transition to the $^5F_5 \rightarrow {}^5I_8$ transition of Ho^{3+} in Lu_2O_3:Yb^{3+}/Ho^{3+}/Eu^{3+} powders as a function of Eu^{3+} doping concentration.

that the monochromaticity of the green UC emission of the powders is improved remarkably by Eu^{3+} doping. The Commission on Illumination (CIE) chromaticity diagram of the samples is presented in Figure S2 in the Supporting Information.

In order to explore the ET mechanism in the Yb^{3+}/Ho^{3+}/Eu^{3+} tridoped system, the decay curves of the Ho^{3+} $^5F_4/^5S_2$ level under 980 nm wavelength excitation were measured first. As shown in Figure 4, the increased Eu^{3+} doping concentration accelerates the decay of the $^5F_4/^5S_2$ level dramatically, demonstrating that the Eu^{3+} doping provides an extra decay pathway for the Ho^{3+} $^5F_4/^5S_2$ level: ET from the $^5F_4/^5S_2$ level of Ho^{3+} to the $^5D_0$ level of Eu^{3+}. Moreover, this phenomenon can also be strongly supported by the occurrence of a $^5D_0 \rightarrow {}^7F_2$ transition of Eu^{3+} in Yb^{3+}/Ho^{3+}/Eu^{3+} tridoped products. However, it is important to point out that, although the ET from the $^5F_4/^5S_2$ level of Ho^{3+} to the $^5D_0$ level of Eu^{3+} is

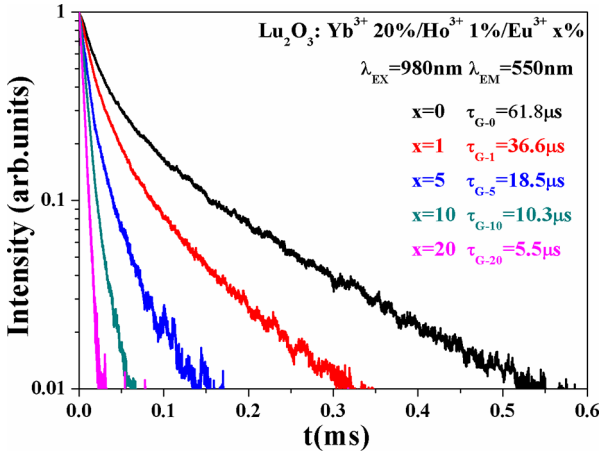

Figure 4. Decay curves of the Ho^{3+} $^5F_4/^5S_2$ level under 980 nm wavelength excitation in Lu_2O_3:Yb^{3+}/Ho^{3+}/Eu^{3+} powders.

effective, the emission intensity of the $^5D_0 \rightarrow {}^7F_2$ transition is very weak, which is due to the low quenching concentration of

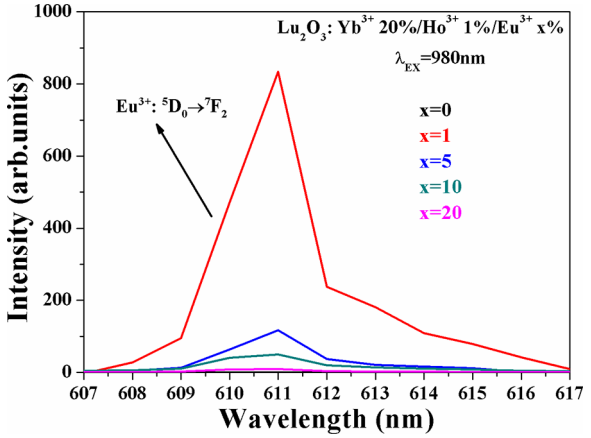

Figure 5. $^5D_0 \rightarrow {}^7F_2$ transition of Eu^{3+} under 980 nm wavelength excitation in Lu_2O_3:Yb^{3+}/Ho^{3+}/Eu^{3+} powders.

Eu^{3+}. As can be seen clearly from Figure 5, the intensity of the $^5D_0 \rightarrow {}^7F_2$ transition gradually weakens with an increase in Eu^{3+} concentration from 1 to 20 mol %, signifying that 1 mol % is the optimal Eu^{3+} doping concentration in this case.

Next, the NIR spectra of the $^5I_6 \rightarrow {}^5I_8$ transition of Ho^{3+} under 980 nm wavelength excitation were detected and are presented in Figure 6. The emission intensity of the $^5I_6 \rightarrow {}^5I_8$ transition is reduced with an increase in Eu^{3+} doping concentration, demonstrating the existence of an ET process from the $^5I_6$ level of Ho^{3+} to Eu^{3+}. In order to further validate this phenomenon, the decay curves of the $^5I_6 \rightarrow {}^5I_8$ transition of Ho^{3+} under 980 nm wavelength excitation were also detected and are shown in Figure 7. Likewise, the decay times of the $^5I_6 \rightarrow {}^5I_8$ transition are decreased from 419.1 to 62.6 μs with an increase in the Eu^{3+} doping concentration, which is further evidence for the ET process from the $^5I_6$ level of Ho^{3+} to Eu^{3+}. On the basis of the above analysis and a combination of the energy level positions of Ho^{3+} and Eu^{3+}, we propose that the ET process is from the $^5I_6$ level of Ho^{3+} to the $^7F_6$ level of Eu^{3+}.[27] In addition, except for the decay curve of the Eu^{3+} undoped sample, all of the decay curves display nonexponential characteristics, resulting from the various ET rates from the $^5I_6$

DOI: 10.1021/acs.inorgchem.7b01236
Inorg. Chem. 2017, 56, 9194−9199

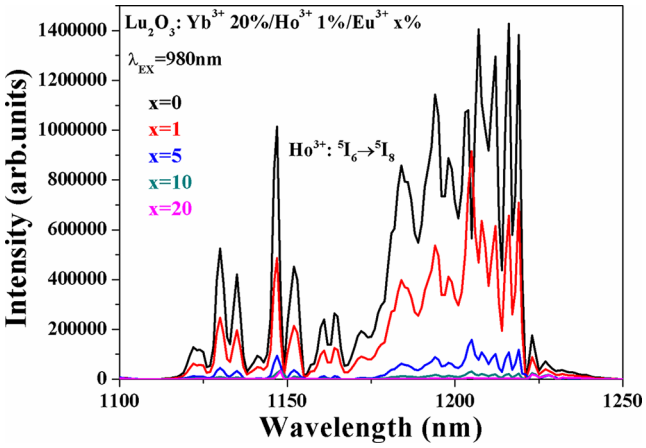

Figure 6. NIR spectra of Lu_2O_3:Yb^{3+}/Ho^{3+}/Eu^{3+} powders with different Eu^{3+} concentrations under 980 nm wavelength excitation.

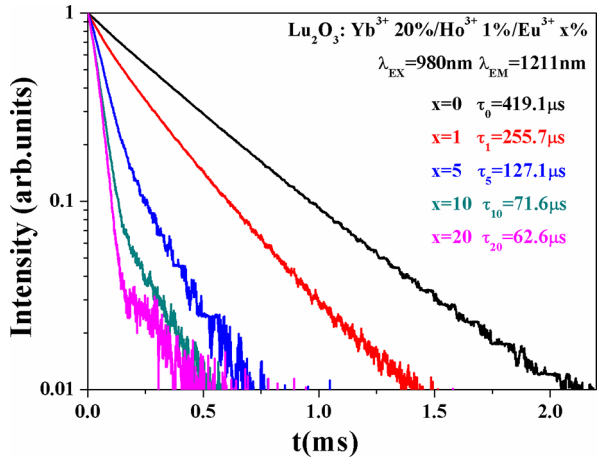

Figure 7. Decay curves of the Ho^{3+} $^5I_6$ level under 980 nm wavelength excitation in Lu_2O_3:Yb^{3+}/Ho^{3+}/Eu^{3+} powders.

level of Ho^{3+} to the $^7F_6$ level of Eu^{3+} caused by nonuniform distribution of Eu^{3+} around the Ho^{3+}.[28]

In the Yb^{3+} and Ho^{3+} codoped system, under 980 nm wavelength excitation at low-output power density, the $^5F_4/^5S_2$ level of Ho^{3+} which produces green emission is mainly populated by the ET process from the Yb^{3+} $^2F_{5/2}$ level to the Ho^{3+} $^5I_6$ level. That is to say, the Eu^{3+} doping not only gives rise to the diminishment of the population of the $^5F_4/^5S_2$ level directly but also results in the decrease in the population of the intermediate $^5I_6$ level. Nevertheless, the integral area ratio of the $^5F_4/^5S_2 \rightarrow {}^5I_8$ transition to the $^5F_5 \rightarrow {}^5I_8$ transition of Ho^{3+} increases obviously, certifying that the Eu^{3+} doping has more influence on the $^5F_5 \rightarrow {}^5I_8$ transition. Before this phenomenon can be explained, it is necessary to carefully analyze the population route of the $^5F_5$ level.

In general, as shown in Figure 8, on excitation by 980 nm wavelength with low-output power density, the considered dominant routes for populating the Ho^{3+} $^5F_5$ level in the Yb^{3+}/Ho^{3+} codoped system include an ET process from the Yb^{3+} $^2F_{5/2}$ level to the Ho^{3+} $^5I_7$ level and a multiphonon relaxation (MPR) process from the upper level Ho^{3+} $^5F_4/^5S_2$. Actually, the Ho^{3+} $^5F_5$ state can also be populated through a cross-relaxation (CR) process between two Ho^{3+} ions: $^5F_4/^5S_2 + {}^5I_7 \rightarrow {}^5F_5 + {}^5I_6$, which has been proposed earlier.[29] In the following paragraphs, the decay curves and luminescence spectra of the

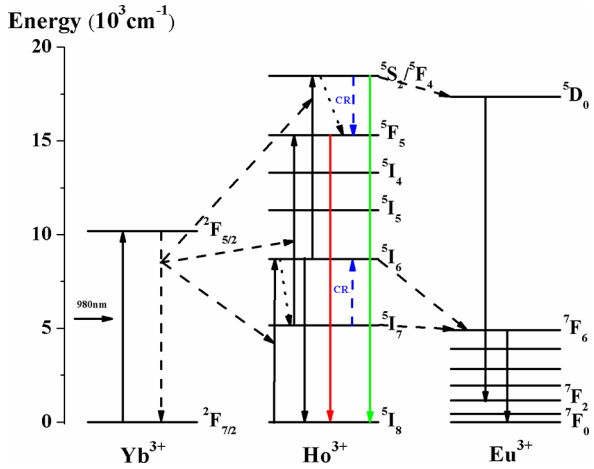

Figure 8. Energy level diagrams of Yb^{3+}, Ho^{3+}, and Eu^{3+} along with the possible ET processes.

related energy levels are utilized to prove the existence of this CR process.

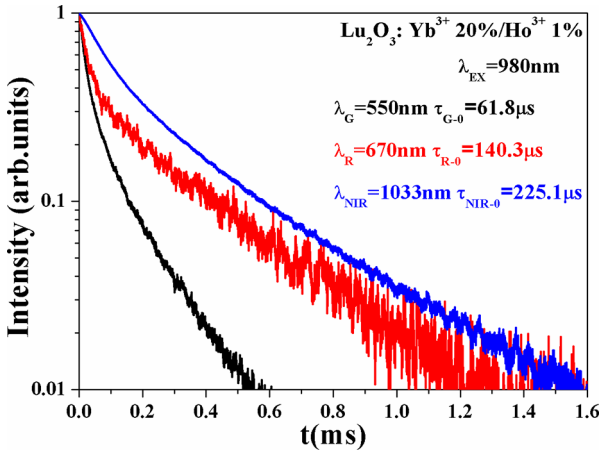

Figure 9. Decay curves of the $^5F_4/^5S_2$ level and the $^5F_5$ level of Ho^{3+} and the $^2F_{5/2}$ level of Yb^{3+} under 980 nm wavelength excitation in Lu_2O_3:Yb^{3+}/Ho^{3+} powders.

Figure 9 shows the decay curves of the $^5F_4/^5S_2$ level and the $^5F_5$ level of Ho^{3+} and the $^2F_{5/2}$ level of Yb^{3+} under 980 nm wavelength excitation in Lu_2O_3:Yb^{3+}/Ho^{3+} powders. The decay time of the Ho^{3+} $^5F_5$ level is between that of the Ho^{3+} $^5F_4/^5S_2$ level and the Yb^{3+} $^2F_{5/2}$ level, which indicates that the population of the Ho^{3+} $^5F_5$ level originates not only from the ET process from the Yb^{3+} $^2F_{5/2}$ level to the Ho^{3+} $^5I_7$ level but also from the contribution of the Ho^{3+} $^5F_4/^5S_2$ level. This can be explained as follows. First, assuming that the population of the Ho^{3+} $^5F_5$ level is mainly contributed by the ET from the lower intermediate Ho^{3+} $^5I_7$ level, then the decay time of the Ho^{3+} $^5F_5$ level should be determined by the decay time of the Ho^{3+} $^5I_7$ level and the Yb^{3+} $^2F_{5/2}$ level simultaneously. However, it is worth noting that the decay time of the Ho^{3+} $^5I_7$ level is much longer than that of the Yb^{3+} $^2F_{5/2}$ level. Therefore, under this hypothesis, the decay time of the Ho^{3+} $^5F_5$ level should be close to the decay time of the Yb^{3+} $^2F_{5/2}$ level. Second, if the contribution of Ho^{3+} $^5F_4/^5S_2$, including the MPR process and CR process is the main approach for populating Ho^{3+} $^5F_5$ level,

DOI: 10.1021/acs.inorgchem.7b01236
Inorg. Chem. 2017, 56, 9194−9199

then as for the MPR process the decay time of the Ho^{3+} $^5F_5$ level should be close to the decay time of the Ho^{3+} $^5F_4/^5S_2$ level; for the CR process between two Ho^{3+} ions in the $^5F_4/^5S_2$ level and $^5I_7$ level, respectively, the decay time of the Ho^{3+} $^5F_5$ level should be determined by the decay time of the Ho^{3+} $^5F_4/^5S_2$ level and Ho^{3+} $^5I_7$ level simultaneously. Considering the extremely long decay time of the Ho^{3+} $^5I_7$ level, the decay time of the Ho^{3+} $^5F_5$ level should be close to the decay time of the Ho^{3+} $^5F_4/^5S_2$ level in this case. In summary, assuming the contribution of the Ho^{3+} $^5F_4/^5S_2$ level is dominant for populating the Ho^{3+} $^5F_5$ level, the decay time of the Ho^{3+} $^5F_5$ level should be close to the decay time of the Ho^{3+} $^5F_4/^5S_2$ level. According to the analysis above with a combination of the test data, it can be proposed that both the ET process from the Yb^{3+} $^2F_{5/2}$ level to the Ho^{3+} $^5I_7$ level and the contribution of the Ho^{3+} $^5F_4/^5S_2$ level contribute to the population of the Ho^{3+} $^5F_5$ level.

As mentioned above, the precondition for the occurrence of a CR process is to obtain the excited Ho^{3+} in the $^5I_7$ level. Meanwhile, it is well-known that, on excitation by 980 nm wavelength in the Yb^{3+}/Ho^{3+} codoped system, the main approach to populate the Ho^{3+} $^5I_7$ level is through an ET process from the Yb^{3+} $^2F_{5/2}$ level to the Ho^{3+} $^5I_6$ level followed by a nonradiative relaxation process. Therefore, in order to separately explore the MPR process from the Ho^{3+} $^5F_4/^5S_2$ level to the Ho^{3+} $^5F_5$ level, the Ho^{3+} singly doped Lu_2O_3 powders were synthesized and the PL spectrum was detected. In PL spectrum measurement, 446 nm wavelength is chosen as the excitation wavelength to excite the Ho^{3+} $^5G_6/^5F_1$ state, from which the Ho^{3+} $^5F_4/^5S_2$ state can be populated by a nonradiative relaxation process. In such a situation, the Ho^{3+} $^5I_7$ state is unable to be populated effectively and then the influence of a CR process can be eliminated. That is to say, the MPR process is the only way to populate the Ho^{3+} $^5F_5$ level. However, as can be seen from Figure 10, the red emission peak

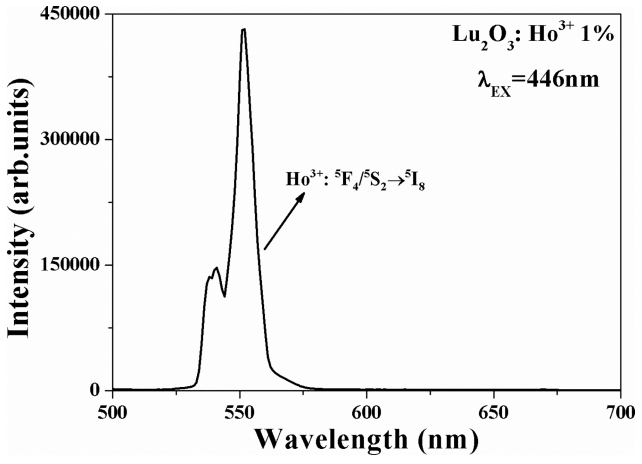

Figure 10. Photoluminescence (PL) spectrum of Lu_2O_3:Ho^{3+} powders excited by 446 nm wavelength.

of the Ho^{3+} $^5F_5 \rightarrow {}^5I_8$ transition disappears, demonstrating that the MPR process is inefficient for populating the Ho^{3+} $^5F_5$ level. Considering that the multiphonon relaxation rate cannot be affected by changing the excitation wavelength, we propose that, under 980 nm wavelength excitation, the contribution of the Ho^{3+} $^5F_4/^5S_2$ level for populating the Ho^{3+} $^5F_5$ level mainly comes from a CR process.

On the basis of the analysis above, it can be concluded that, upon 980 nm wavelength excitation, the population of the Ho^{3+} $^5F_5$ level in the Yb^{3+}/Ho^{3+} codoped system is mainly through an ET process from the Yb^{3+} $^2F_{5/2}$ level to the Ho^{3+} $^5I_7$ level and a CR process between two Ho^{3+} ions in the $^5F_4/^5S_2$ level and $^5I_7$ level, respectively. Interestingly, the Ho^{3+} $^5I_7$ level participates in both of the two processes as the intermediate level. In the $Yb^{3+}/Ho^{3+}/Eu^{3+}$ tridoped system, the energy level gap between the Ho^{3+} $^5I_7$ level and the Ho^{3+} $^5I_8$ level matches well with that between the Eu^{3+} $^7F_6$ level and Eu^{3+} $^7F_0$ level. Thus, the Ho^{3+} in the $^5I_7$ level can easily transfer its energy to the Eu^{3+} in the ground state, resulting in the population of the Eu^{3+} $^7F_6$ level and a decrease in red emission intensity. Since this ET process is almost resonant, it is more efficient than the ET from the Ho^{3+} $^5F_4/^5S_2$ level to the Eu^{3+} $^5D_0$ level as well as the ET from the Ho^{3+} $^5I_6$ level to the Eu^{3+} $^7F_6$ level, as reported previously.[27] Therefore, it is for this reason that the integral area ratio of green emission to red emission of Ho^{3+} increases distinctly.

CONCLUSIONS

In summary, the improvement of green UC emission monochromaticity of Lu_2O_3:Yb^{3+}/Ho^{3+} powders has been realized by tridoping Eu^{3+}. As the Eu^{3+} doping concentration is increased from 0 to 20 mol %, the integral area ratio of green emission to red emission of Ho^{3+} increases 4.3-fold. The steady state fluorescence spectra and the decay curves have been utilized to demonstrate the ET from the Ho^{3+} $^5F_4/^5S_2$ level to the Eu^{3+} $^5D_0$ level along with the ET from the Ho^{3+} $^5I_6$ level to the Eu^{3+} $^7F_6$ level. In addition, the population routes of the red-emitting Ho^{3+} $^5F_5$ level in the Yb^{3+}/Ho^{3+} codoped system under 980 nm wavelength excitation have also been explored. The results show that the main approaches for populating the Ho^{3+} $^5F_5$ level are the ET process from the Yb^{3+} $^2F_{5/2}$ level to the Ho^{3+} $^5I_7$ level and the CR process between two nearby Ho^{3+} ions in the $^5F_4/^5S_2$ level and $^5I_7$ level, respectively. The MPR process originating from the Ho^{3+} $^5F_4/^5S_2$ level is useless to populate the Ho^{3+} $^5F_5$ level. Since there is a good match between the Ho^{3+} $^5I_7$ level and Eu^{3+} $^7F_6$ level, the energy of the Ho^{3+} $^5I_7$ level can be easily transferred t theo Eu^{3+} $^7F_6$ level by an approximate resonant ET process, resulting in a serious decrease in the red UC emission intensity. Although the Eu^{3+} doping reduces the intensity of green UC emission, an improvement in the integral area ratio of green emission to red emission of Ho^{3+} has been realized, which is due to the much higher efficiency of the ET from the Ho^{3+} $^5I_7$ level to the Eu^{3+} $^7F_6$ level in comparison with the ET from the Ho^{3+} $^5F_4/^5S_2$ level to the Eu^{3+} $^5D_0$ level and the ET from the Ho^{3+} $^5I_6$ level to the Eu^{3+} $^7F_6$ level.

ASSOCIATED CONTENT

Supporting Information

The Supporting Information is available free of charge on the ACS Publications website at DOI: 10.1021/acs.inorgchem.7b01236.

UC spectra and CIE chromaticity diagram of Lu_2O_3:$Yb^{3+}/Ho^{3+}/Eu^{3+}$ powders with different Eu^{3+} concentrations (PDF)

AUTHOR INFORMATION

Corresponding Authors

*E-mail for G.X.: xianggt@cqupt.edu.cn.

DOI: 10.1021/acs.inorgchem.7b01236
Inorg. Chem. 2017, 56, 9194−9199

*E-mail for J.Z.: zhangjh@ciomp.ac.cn.

ORCID

Guotao Xiang: 0000-0003-3587-6654

Notes

The authors declare no competing financial interest.

■ ACKNOWLEDGMENTS

This work was financially supported by the National Natural Science Foundation of China (11674044), the Chongqing Research Program of Basic Research and Frontier Technology (CSTC2017jcyjAX0046), and the Science and Technology Research Program of Chongqing Municipal Education Commission (KJ1704071).

■ REFERENCES

(1) Xiang, G. T.; Zhang, J. H.; Hao, Z. D.; Zhang, X.; Pan, G. H.; Luo, Y. S.; Lü, W.; Zhao, H. F. Importance of Suppression of Yb^{3+} De-Excitation to Upconversion Enhancement in β-$NaYF_4$: Yb^{3+}/Er^{3+}@β-$NaYF_4$ Sandwiched Structure Nanocrystals. *Inorg. Chem.* **2015**, *54*, 3921−3928.

(2) Suo, H.; Guo, C. F.; Wang, W. B.; Li, T.; Duan, C. K.; Yin, M. Mechanism and stability of spectrally pure green up-conversion emission in Yb^{3+}/Ho^{3+} co-doped $Ba_5Gd_8Zn_4O_{21}$ phosphors. *Dalton Trans.* **2016**, *45*, 2629−2636.

(3) Zhao, C. Z.; Kong, X. G.; Liu, X. M.; Tu, L. P.; Wu, F.; Zhang, Y. L.; Liu, K.; Zeng, Q. H.; Zhang, H. Li^+ ion doping: an approach for improving the crystallinity and upconversion emissions of $NaYF_4$: Yb^{3+}, Tm^{3+} nanoparticles. *Nanoscale* **2013**, *5*, 8084−8089.

(4) Li, Z. Q.; Zhang, Y.; Jiang, S. Multicolor Core/Shell-Structured Upconversion Fluorescent Nanoparticles. *Adv. Mater.* **2008**, *20*, 4765−4769.

(5) Johnson, N. J. J.; Korinek, A.; Dong, C. H.; van Veggel, F. C. J. M. Self-Focusing by Ostwald Ripening: A Strategy for Layer-by-Layer Epitaxial Growth on Upconverting Nanocrystals. *J. Am. Chem. Soc.* **2012**, *134*, 11068−11071.

(6) Barreto, J. A.; O'Malley, W.; Kubeil, M.; Graham, B.; Stephan, H.; Spiccia, L. Nanomaterials: applications in cancer imaging and therapy. *Adv. Mater.* **2011**, *23*, H18−H40.

(7) Wang, Y. F.; Sun, L. D.; Xiao, J. W.; Feng, W.; Zhou, J. C.; Shen, J.; Yan, C. H. Rare-Earth Nanoparticles with Enhanced Upconversion Emission and Suppressed Rare-Earth-Ion Leakage. *Chem. - Eur. J.* **2012**, *18*, 5558−5564.

(8) Gnach, A.; Lipinski, T.; Bednarkiewicz, A.; Rybka, J.; Capobianco, J. A. Upconverting nanoparticles: assessing the toxicity. *Chem. Soc. Rev.* **2015**, *44*, 1561−1584.

(9) Mehrabani, S.; Armani, A. M. Blue upconversion laser based on thulium-doped silica microcavity. *Opt. Lett.* **2013**, *38*, 4346−4349.

(10) Wang, Y. F.; Liu, G. Y.; Sun, L. D.; Xiao, J. W.; Zhou, J. C.; Yan, C. H. Nd^{3+} Sensitized Upconversion Nanophosphors: Efficient In Vivo Bioimaging Probes with Minimized Heating Effect. *ACS Nano* **2013**, *7*, 7200−7206.

(11) Lucky, S. S.; Idris, N. M.; Li, Z. Q.; Huang, K.; Soo, K. C.; Zhang, Y. Titania Coated Upconversion Nanoparticles for Near-Infrared Light Triggered Photodynamic Therapy. *ACS Nano* **2015**, *9*, 191−205.

(12) Chan, E. M.; Han, G.; Goldberg, J. D.; Gargas, D. J.; Ostrowski, A. D.; Schuck, P. J.; Cohen, B. E.; Milliron, D. J. Combinatorial Discovery of Lanthanide-Doped Nanocrystals with Spectrally Pure Upconverted Emission. *Nano Lett.* **2012**, *12*, 3839−3845.

(13) Zeng, S. J.; Yi, Z. G.; Lu, W.; Qian, C.; Wang, H. B.; Rao, L.; Zeng, T. M.; Liu, H. R.; Liu, H. J.; Fei, B.; Hao, J. H. Simultaneous Realization of Phase/Size Manipulation, Upconversion Luminescence Enhancement, and Blood Vessel Imaging in Multifunctional Nanoprobes Through Transition Metal Mn^{2+} Doping. *Adv. Funct. Mater.* **2014**, *24*, 4051−4059.

(14) Sheng, Y. Q.; Xu, L. L.; Liu, J.; Zhai, D.; Zhang, Z. G. Improving monochromaticity of upconversion luminescence by codoping Eu^{3+} ions in Y_2O_3:Ho^{3+}, Yb^{3+} nanocrystals. *J. Lumin.* **2010**, *130*, 338−341.

(15) Wei, Y.; Lu, F. Q.; Zhang, X. R.; Chen, D. P. Synthesis of Oil-Dispersible Hexagonal-Phase and Hexagonal-Shaped $NaYF_4$:Yb, Er Nanoplates. *Chem. Mater.* **2006**, *18*, 5733−5737.

(16) Krämer, K. W.; Biner, D.; Frei, G.; Güdel, H. U.; Hehlen, M. P.; Lüthi, S. R. Hexagonal Sodium Yttrium Fluoride Based Green and Blue Emitting Upconversion Phosphors. *Chem. Mater.* **2004**, *16*, 1244−1251.

(17) Xiang, G. T.; Zhang, J. H.; Hao, Z. D.; Zhang, X.; Luo, Y. S.; Lü, S. Z.; Zhao, H. F. Transition to cubic phase and enhancement of green upconversion emission by adding La^{3+} ions in hexagonal $NaLuF_4$:Yb^{3+}/Er^{3+} nanocrystals. *CrystEngComm* **2014**, *16*, 2499−2507.

(18) Dong, B.; Cao, B. S.; He, Y. Y.; Liu, Z.; Li, Z. P.; Feng, Z. Q. Temperature Sensing and In Vivo Imaging by Molybdenum Sensitized Visible Upconversion Luminescence of Rare-Earth Oxides. *Adv. Mater.* **2012**, *24*, 1987−1993.

(19) Li, J.; Zhang, J. H.; Hao, Z. D.; Zhang, X.; Zhao, J. H.; Luo, Y. S. Intense upconversion luminescence and origin study in Tm^{3+}/Yb^{3+} codoped calcium scandate. *Appl. Phys. Lett.* **2012**, *101*, 121905.

(20) Li, T.; Guo, C. F.; Yang, Y. M.; Li, L.; Zhang, N. Efficient green up-conversion emission in Yb^{3+}/Ho^{3+} co-doped $CaIn_2O_4$. *Acta Mater.* **2013**, *61*, 7481−7487.

(21) Etchart, I.; Huignard, A.; Bérard, M.; Nordin, M. N.; Hernández, I.; Curry, R. J.; Gillind, W. P.; Cheetham, A. K. Oxide phosphors for efficient light upconversion: Yb^{3+} and Er^{3+} co-doped Ln_2BaZnO_5 (Ln = Y, Gd). *J. Mater. Chem.* **2010**, *20*, 3989−3994.

(22) Page, R. H.; Schaffers, K. I.; Waide, P. A.; Tassano, J. B.; Payne, S. A.; Krupke, W. F. Upconversion-pumped luminescence efficiency of rare-earth-doped hosts sensitized with trivalent ytterbium. *J. Opt. Soc. Am. B* **1998**, *15*, 996−1008.

(23) Li, Y. P.; Zhang, J. H.; Zhang, X.; Luo, Y. S.; Ren, X. G.; Zhao, H. F.; Wang, X. J.; Sun, L. D.; Yan, C. H. Near-Infrared to Visible Upconversion in Er^{3+} and Yb^{3+} Codoped Lu_2O_3 Nanocrystals: Enhanced Red Color Upconversion and Three-Photon Process in Green Color Upconversion. *J. Phys. Chem. C* **2009**, *113*, 4413−4418.

(24) Capobianco, J. A.; Vetrone, F.; Boyer, J. C.; Speghini, A.; Bettinelli, M. Visible upconversion of Er^{3+} doped nanocrystalline and bulk Lu_2O_3. *Opt. Mater.* **2002**, *19*, 259−268.

(25) He, E. J.; Zheng, H. R.; Gao, W.; Tu, Y. X.; Lu, Y.; Li, G. A. Investigation of upconversion and downconversion fluorescence emissions from β-$NaLn1F_4$:Yb^{3+}, $Ln2^{3+}$ (Ln1 = Y, Lu; Ln2 = Er, Ho, Tm, Eu) hexagonal disk system. *Mater. Res. Bull.* **2013**, *48*, 3505−3512.

(26) Xiang, G. T.; Zhang, J. H.; Hao, Z. D.; Zhang, X.; Pan, G. H.; Chen, L.; Luo, Y. S.; Lü, S. Z.; Zhao, H. F. Solvothermal synthesis and upconversion properties of about 10 nm orthorhombic LuF_3: Yb^{3+}, Er^{3+} rectangular nanocrystals. *J. Colloid Interface Sci.* **2015**, *459*, 224−229.

(27) Zhang, H. L.; Sun, D. L.; Luo, J. Q.; Chen, J. K.; Yang, H. J.; Xiao, J. Z.; Zhang, Q. L.; Yin, S. T. Growth, thermal, and spectroscopic properties of a Cr,Yb,Ho,Eu:YAP laser crystal. *Opt. Mater.* **2014**, *36*, 1361−1365.

(28) Xiang, G. T.; Zhang, J. H.; Hao, Z. D.; Zhang, X.; Pan, G. H.; Luo, Y. S.; Lü, S. Z.; Zhao, H. F. *Phys. Chem. Chem. Phys.* **2014**, *16*, 9289−9293.

(29) Tang, M. M.; Wang, X. S.; Peng, D. F.; Wang, W.; Sun, H. Q.; Yao, X. Strong green and red up-conversion emission in Ho^{3+}, Yb^{3+} and Li^+ co- or tri-doped $SrAl_2O_4$ ceramics. *J. Alloys Compd.* **2012**, *529*, 49−51.

DOI: 10.1021/acs.inorgchem.7b01236
Inorg. Chem. 2017, 56, 9194−9199